

# Event-Based Imaging of Levitated Microparticles

**Yugang Ren<sup>\*1</sup>, Enrique Benedetto<sup>\*1</sup>, Harry Borrill<sup>1</sup>, Yelizaveta Savchuk<sup>1</sup>, Molly Message<sup>1</sup>, Katie O’Flynn<sup>1</sup>, Muddassar Rashid<sup>1</sup>, James Millen<sup>1,2</sup>**

<sup>1</sup>Department of Physics, King’s College London, Strand, London, WC2R 2LS, UK.

<sup>2</sup>London Centre for Nanotechnology, Department of Physics, King’s College London, Strand, London, WC2R 2LS, UK.

E-mail: [james.millen@kcl.ac.uk](mailto:james.millen@kcl.ac.uk)

\* Joint first authors

23 June 2022

**Abstract.** Event-based imaging is a neurmorphic detection technique whereby an array of pixels detects a positive or negative change in light intensity at each pixel, and is hence particularly well suited to detecting motion. As compared to standard camera technology, an event-based camera reduces redundancy by not detecting regions of the image where there is no motion, allowing increased frame-rates without compromising on field-of-view. Here, we apply event-based imaging to detect the motion of a microparticle levitated under vacuum conditions, which greatly facilitates the study of nano-thermodynamics and enables the independent detection and control of arrays of many particles.

## 1. Introduction

When unravelling the underlying physics of particles interacting with external forces, or of interacting multi-particle systems, object tracking is key. One must consider a range of detection metrics such as field-of-view, resolution, latency, sensitivity, bandwidth, signal-to-noise ratio (SNR) and the ability to detect multiple objects.

In this work, we consider tracking the motion of microparticles levitated under vacuum conditions by optical, electrical or magnetic fields [1, 2]. Such systems are of interest for studies of fundamental quantum science [3], nano-thermodynamics [4] and advanced sensing [5, 6].

When working with particles optically trapped in liquid, it is sufficient to use standard CMOS or CCD cameras to track their motion, since the viscous damping provided by the liquid reduces dynamical timescales to a level suitable for camera framerates. However, once objects are levitated in vacuum, their motion is underdamped and faster tracking is required [7]. Although this is possible at the 100 kHz level with expensive high-speed

CMOS cameras [8], this requires significant reduction in the sensor resolution. Hence, particle tracking is usually performed using photodiodes, balanced photodetectors or quadrant photodetectors. Whilst these devices are fast, even tracking at GHz rates [9, 10], they have limited field-of-view, restricting tracking to scales not much larger than the optical wavelength. This can limit studies of nanothermodynamics or nonlinear motion where particles may explore large regions of space [3].

Additionally, a key technique when working with levitated objects is the application of real-time feedback onto their motion. This has enabled cooling to the quantum ground state of a harmonic potential [11], but more generally is essential for stabilization under vacuum conditions. Balanced photodetectors are the standard tool to realise real-time feedback [12], although recent work employing powerful graphics cards with limited number of pixels [13] or on-board microprocessors [14] has enabled feedback control of sub-500 Hz oscillators via CMOS camera detection. We also note that cameras have excellent SNR and allow super-resolution detection [13], allowing one to minimize the amount of light required to detect levitated particles avoiding absorption [15] and photon recoil heating [16].

Finally, the prospect of levitating systems of multiple interacting particles has emerged [2], for distributed sensing [17] or generation of entanglement [18]. Single photodetectors can only track single particles, whereas cameras are well suited to multi-particle detection.

Conventional, CMOS/CCD based cameras work using a specified region of interest (ROI) or the whole pixel array to capture light from a scene. An alternative approach is that of event-based imaging (EBI), where pixels work independently of each other, triggering only when the change in light intensity is above a preset threshold [19]. This enables a dynamic ROI, thus enabling decreased informational load compared to conventional cameras. The motion captured is also novel, in that a unperturbed image will be undetected by the camera and only movement is captured.

In this paper, we apply EBI for detecting the motion of microparticles levitated in vacuum. This imaging technique offers the potential for tracking single and multiple objects, whilst an integrated tracking algorithm provides the real-time position of each object for use in feedback for state control. To the best of our knowledge, it is the first such application of EBI to trapped particles in any medium.

## 2. Principles of Event-based detection

Conventional cameras, such as CMOS/CCD, capture continuous movement as a sequence of still images (frames). This frame-based approach generates a time discretization of the movement, given by the inverse of the frame rate. Each frame is produced

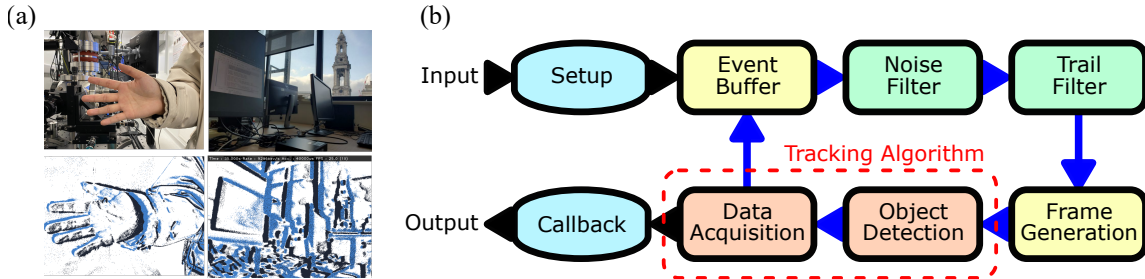


Figure 1: (a) Upper images are taken with a conventional CMOS camera, lower images are taken by an event-based camera (EBC). The black and blue pixels in the EBC image correspond to negative / positive changes in light intensity, respectively. (b) Information pipeline from the point of data captured by the EBC camera and then processed into positional information.

by a synchronous response to the light received from all the pixels in the sensor, resulting in a common frame rate for the entire scene. As a result, stationary elements are unnecessarily replicated, while moving elements are under sampled [20].

Event-based imaging (EBI) provides a novel approach to image acquisition by only capturing changes in images through the detection of modifications in light intensity on each pixel [19]. Pixels in these neuromorphic sensors (sensors that try to mimic the neural structure of the brain) are completely independent. Each one of them contains a contrast detector (CD) that continuously tracks photocurrents. When the variation of a photocurrent crosses a threshold, the CD triggers a contrast detection event, which represents a relative increase (positive) or decrease (negative) in light intensity. It then initiates the measurement of a new value, as outlined in fig. 1(b). Pixels which do not observe changes in light intensities that exceed the threshold do not produce output. As a result, there is a suppression of temporal redundancy, and since each pixel is independent and asynchronous, there is no time discretization from frame-based acquisition techniques.

This can be easily seen in fig. 1(a) where two images obtained with different cameras are shown. The event-based image was obtained by gently moving the camera, triggering the CD associated to the corresponding pixels. The output image consists of only three colours: white pixels indicate no change in light intensity across the threshold; blue and black pixels represent positive and negative changes in light intensity across the threshold, respectively. Only the blue and black pixels are transmitted as data. By comparing both sets of images in fig. 1(a), it is therefore clear that the amount of data transferred is suppressed with EBI.

In conventional cameras the bandwidth of the communication link is usually a constraint whenever higher acquisition rates are needed to track rapid movement. This leads users

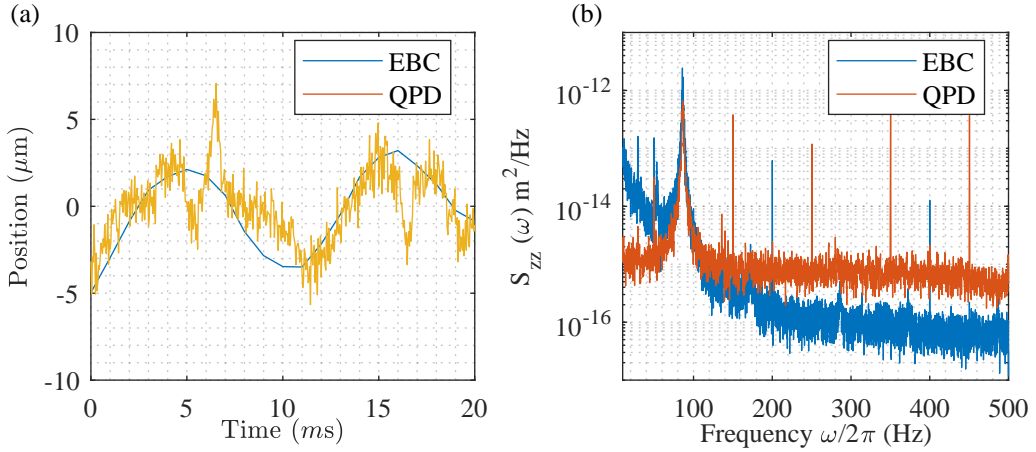


Figure 2: (a) Time domain motion of one degree-of-freedom of a levitated microparticle, obtained via the GTA of an EBC (blue) and via a QPD (red). (b) Corresponding PSDs, illustrating the varying noise characteristics of the two detection methods.

to reduce the region of interest (ROI) of the sensor to decrease the amount of data per frame [13]. Due to the suppression of data redundancy, the data volume transmitted by the event-based camera is considerably reduced, allowing acquisition rates over 1 GHz [19].

### 2.1. Particle tracking with event-based imaging

Figure 1(b) shows the detailed process of tracking based on EBI. All the input information related to camera sensors are read initially and in the setup period, camera sensor parameters are tuned. An event producer, which is contained in the event buffer, is used to generate a stream of events. For each stream of events, a noise filter is applied at first to pick up events in the neighboring 8 pixels during a certain time. A trail filter is then employed to accept an event if the last event is detected at the same position within an accumulation time. All of the data collected by the sensor pixels generates a frame and a generic tracking algorithm (GTA) analyzes these frames to extract detected objects and associate data to previous frames. When the detected object is recognized, there is a trigger in callback and the motional information of detected particle is obtained from output.

Figure 2(a) shows the output from the GTA of an event-based camera (EBC) ‡, compared to the output of a quadrant photodiode (QPD) §, when tracking the oscillatory motion of a microparticle. Figure 2(b) shows the corresponding derived power spectral densities of the particle motion. Like all balanced detection methods, the QPD min-

‡ Prophesee Evaluation Kit Gen3M VGA CD 1.1

§ New Focus 2901 Quadrant Cell Photoreceiver

imizes  $1/f$  noise at low frequencies, whereas the EBC has lower-noise performance at higher frequencies.

### 3. Experimental system

Charged silica microspheres of diameter  $5\ \mu\text{m}$  and charge  $Q$  are levitated in partial vacuum using a Paul trap, made with four 3mm-diameter rods and two 1mm-diameter endcap rods (not shown, aligned axially along the centre of the structure), as illustrated in fig. 3(a). The microsphere is trapped using an oscillating electric field with frequency  $\Omega_{RF} = 2\pi \times 800\ \text{rad s}^{-1}$  and amplitude  $V_{RF} = 750\ \text{V}$ . The two endcap electrodes are held at -4V DC. The particles are loaded into the Paul trap using laser-induced acoustic desorption (LIAD) [21, 22] at a pressure of  $2 \times 10^{-2}\ \text{mbar}$ .

An illumination laser (532 nm) is focused onto the trapped particle, with a beam waist of  $\sim 80\ \mu\text{m}$ . The scattered light is collected by a microscope and directed onto an event-based camera (EBC) or QPD for motion detection. In fig. 3(b) we show the signal-to-noise ratio (SNR) of the motional frequency in the PSD (as shown in fig.2(b)) as recorded by the EBC, as we vary the power of the illumination laser. We estimate the maximal scattered power reaching the EBC sensor, illustrating the excellent sensitivity of the detector.

#### 3.1. Calibration Methods

Regardless of the detection method used, the detector has to be calibrated. Here we compare the EBC to a QPD. The motion of the particle is calibrated by applying a known potential difference  $\Delta U$  across the endcap electrodes, causing the particle to move in the  $z$ -direction. The particle oscillates at the centre of the trap when  $\Delta U = 0\ \text{V}$ . If the voltage of one of the endcaps is modified from  $U_0 \rightarrow U_1$ , the resulting voltage difference  $\Delta U = U_1 - U_0$  exerts a force on the particle  $\vec{F} = F_z \hat{z}$ , where  $\hat{z}$  denotes a unit vector along the  $z$ -axis, determined by:

$$F_z = \frac{Q \Delta U}{d}, \quad (1)$$

where  $d$  is the distance between the endcap electrodes. Since the Paul trap provides a harmonic pseudo-potential, the particle also experiences a linear restoring force:

$$F_z = -k \langle z \rangle, \quad (2)$$

where  $k$  is the trap stiffness and  $\langle z \rangle$  is the average position of the particle in the axial axis (assuming  $\langle z \rangle = 0$  when  $\Delta U = 0$ ).

Noting that the measured  $\langle z_m \rangle$  is in volts for the QPD, and pixels for the EBC, and related to true value of  $\langle z \rangle$  through a conversion factor  $\gamma$ , with units V/m and pixels/m,

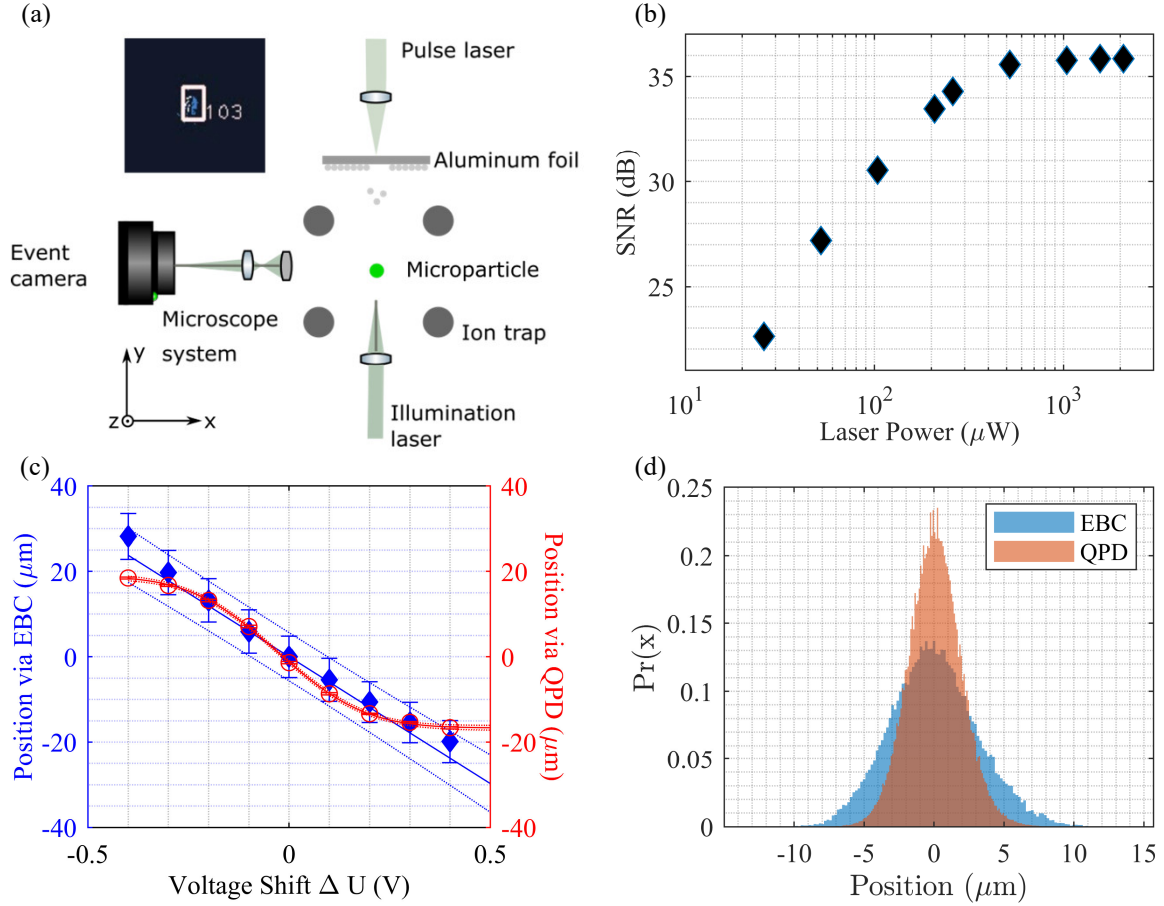


Figure 3: (a) Schematic overview of experimental setup. Single silica microspheres are levitated in a Paul trap, illuminated by a laser, and the scattered light is imaged onto an EBC. The inset shows a typical image captured by the EBC. (b) EBC SNR at the motional frequency of the levitated microparticle, as a function of the maximal scattered laser power reaching the detector. (c) Average position of a levitated microparticle in response to a potential difference across the endcap electrodes. It is evident that the response of the EBC (blue) is linear across the full range of motion, whereas the QPD (red) responds non-linearly at large displacements. (d) Position probability histogram for the motion of a levitated microparticle, recorded by the EBC (blue) and QPD (red), where it is evident that the QPD cannnot pick up large displacements.

respectively, we can equation these two equations. Considering further that  $k = m\omega_z^2$  for a harmonic oscillator of mass  $m$  and oscillation frequency  $\omega_z$ , then:

$$\langle z_m \rangle = -\gamma \frac{Q}{m} \frac{\Delta U}{d\omega_z^2}. \quad (3)$$

By measuring the mean displacement of the particle for a given force applied through a potential difference across the endcap electrodes we can determine the conversion factor  $\gamma$  for the detector. The oscillator frequency can be obtained from the power spectral density of the time trace (fig. 2) and  $Q/m$  obtained by solving the Mathieu equations

(see Appendix A). In our system we typically trap particles of charge  $Q = 2 \times 10^4 e$ .

The calibrated particle position as a response to a potential difference can be seen in fig. 3(c). It is apparent that as  $|\Delta U|$  becomes large, the response of the QPD becomes nonlinear, whereas eqn. (3) predicts a linear response. This can be somewhat mitigated through a nonlinear calibration (see Appendix B), but limits the field-of-view of the QPD. On the other hand, the EBC has a linear response to the particle displacement across the full range. Figure 3(d) shows a histogram of the equilibrium motion of the trapped particle, again showing that large displacements are missing when using the QPD. Hence, we can track both small (i.e. the oscillatory motion) and large displacements using EBI.

## 4. Applications in Optomechanics

### 4.1. Non-equilibrium Physics

Levitated particles provide an ideal system for probing stochastic thermodynamics [4]. This is in part due to the characteristic energy of the system being comparable to that of thermal fluctuations of the bath, which enable levitated systems to be highly sensitive to surrounding fluctuations. The coupling to the bath is characterized by the ratio of its oscillation frequency  $\omega_z$  to its momentum damping rate  $\Gamma$ , yielding overdamped ( $\Gamma \gg \omega_z$ ) and underdamped ( $\Gamma \ll \omega_z$ ) regimes. In the overdamped regime, trapped particles have been used for studying heat engines [23], non-thermal baths [24], and for testing Landauer's principle [25]. In the underdamped regime, the studies in stochastic thermodynamics have been extended to observing Kramer's turnover [26], studying non-equilibrium Landauer's principle [27] and testing fluctuation-dissipation theorems [28].

Often when such systems exhibit non-equilibrium dynamics, they go beyond the linear detection regime of photodiode-based detection systems, and CMOS cameras would need a large ROI to capture the dynamics, at the expense of bandwidth.

EBI employs a dynamic ROI, based on only triggered pixels. To characterise the capability of EBI, and the GTA of the EBC, we cause random jumps in the particles' position with varying time intervals,  $\tau$  (see supplementary Appendix C). These random jumps, as seen in fig. 4(a), are driven by voltage changes applied to the endcap electrodes which follow telegraph noise statistics (see supplementary Appendix C) distributed about a mean waiting time  $\bar{\tau}$ . For fast switching times relative to the gas damping rate  $\Gamma_0$ , the position probability distribution of the particle is Gaussian, and for slow switching times it is bimodal, as shown in fig. 4(b). Comparing to fig. 3(c), the particle's motion would go deep into the nonlinear range of the QPD. However, the EBC has no such limitation,

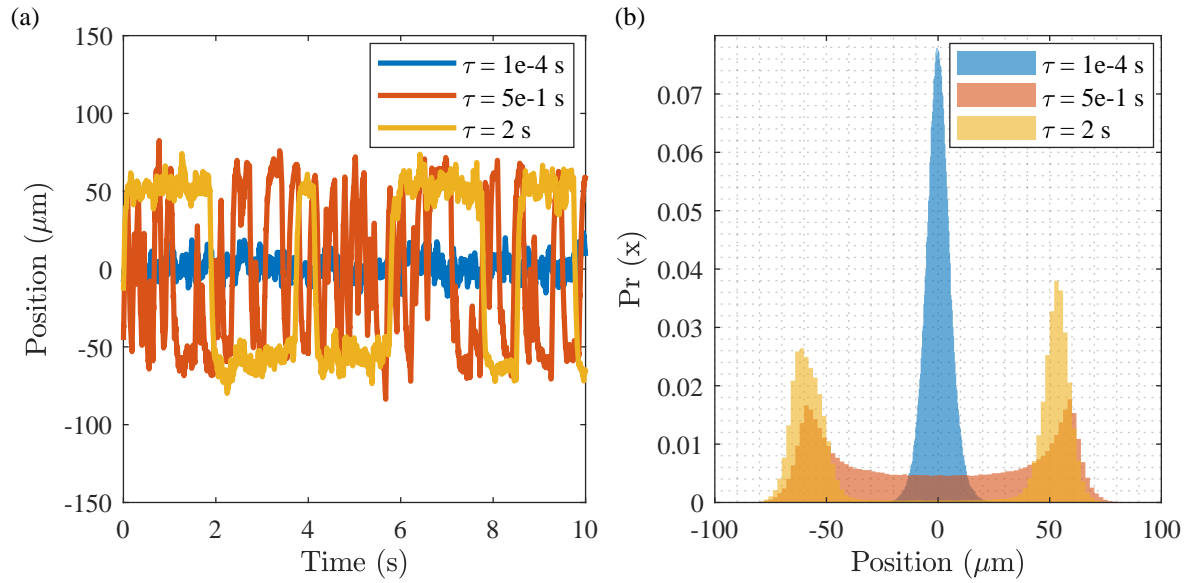


Figure 4: (a) EBC particle tracking when it is driven to make large random jumps in its equilibrium position. Blue, red and yellow lines indicate different jump time-constants  $\tau$ . (b) Position probability distributions for different jump time-constants. As predicted, when  $\tau = 1 \times 10^{-4} \text{ s}$ , the distribution is Gaussian, and for slower jump time-constants the distribution is bimodal.

and position shifts greater than  $50 \mu\text{m}$  are tracked.

The limiting factor for the EBC is the GTA, which is not a general limitation of EBI. For shifts in position that are in quick succession and large in displacement, the GTA lags behind or misses consecutive shifts. This is illustrated in fig. 4(a), where the GTA of the EBC faithfully tracks the particle position when  $\bar{\tau} > 1 \text{ s}$ . For shorter mean waiting times,  $\bar{\tau} < 500 \text{ ms}$  the GTA struggles to track the jumps, as evidenced by apparent spikes in the time domain signal.

This lag in tracking by the GTA is a consequence of numerous filters applied to be able to track arbitrary object trajectories. The underlying dynamics are well known for levitated particles in this regime, therefore a more precise filter, like an asynchronous Kalman filter [29] in which we can input the expected equation of motion, will enable more accurate tracking of fast large shifts. Such filters are currently being explored in the literature for tracking space satellites or various celestial bodies, the trajectories of which are well known [30]. Again, the GTA doesn't represent a true limit to EBI and, as shown in fig. 4(b), the EBC used in this study can simultaneously track large displacements and the smaller oscillations of the particle about its equilibrium position.

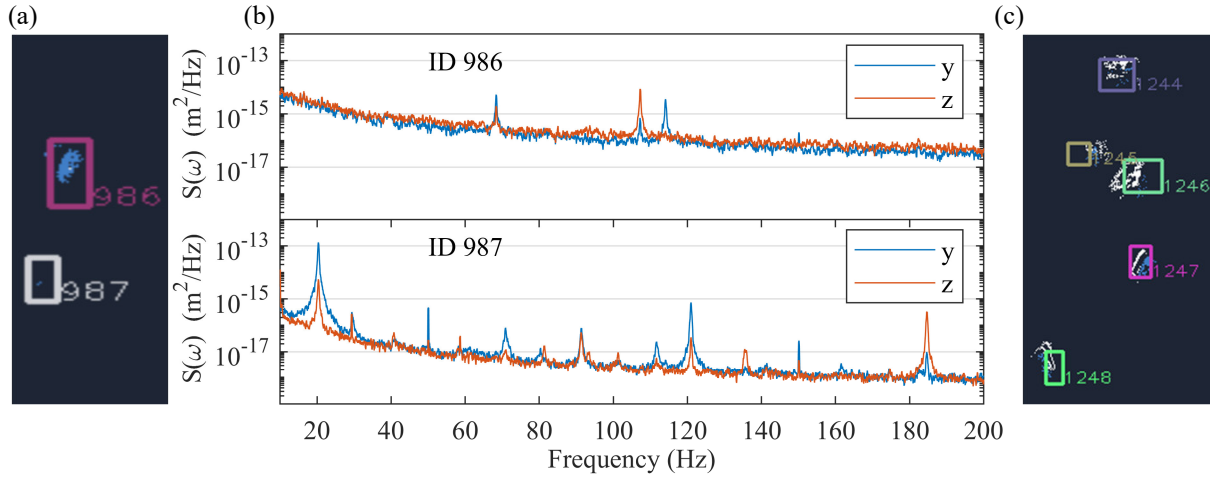


Figure 5: (a) EBC image of two microspheres, with the boxes indicating that the GTA has identified them as two separate objects to track, labelled "986" and "987". (b) PSDs of the motion of these two microspheres. (c) EBC image of five microspheres, with the boxes indicating that the GTA has identified them as five separate objects to track.

#### 4.2. Multi-Particle Tracking

We extend our study to multi-particle tracking using EBI. The ability to track arrays of particles would enable the study of quantum correlations [31, 32, 33, 34], non-hermitian systems [35], and the detection of dark matter [36, 37], vacuum friction [38] and differential force-sensing [39]. To date, few have explored the multi-particle regime experimentally, with only two particles trapped to demonstrate state-swapping and sympathetic cooling [40], dipole-dipole [41, 42] and coulomb-coulomb [43] interactions, and cold damping and state control [44].

Motional detection of individual particles in a multiple particle trap is a non-trivial problem. A single focused light beam can carry motional information of two particles [45], or an additional beam can be added for detection of the second particle [41]. Going beyond two particles in this way would require a complex and non-scalable optical setup. Within the context of optical tweezers, there are numerous approaches most suited to tracking multiple particles, using high-speed cameras [46] and multiple-beams in conjunction with a QPD [47], but these detection methods face the same limitation outlined earlier in this paper.

Figure 5(a) shows an image of two microspheres of  $5\ \mu\text{m}$  diameter trapped in a Paul trap, captured on our EBC. The image shows the bounding boxes which the GTA uses to track the two-dimensional position of the particles, labelled "986" and "987".

The levitated microspheres are tracked and their motional information separately reconstructed in fig. 5(b). We observe oscillation frequencies of both particles indepen-

dently. For particle ID 986, the motional frequencies are  $\{\omega_x^{986} = 2\pi \times 68 \text{ rad s}^{-1}, \omega_y^{986} = 2\pi \times 114 \text{ rad s}^{-1}, \omega_z^{986} = 2\pi \times 108 \text{ rad s}^{-1}\}$ , whilst particle ID 987 has frequencies  $\{\omega_x^{987} = 2\pi \times 20 \text{ rad s}^{-1}, \omega_y^{987} = 2\pi \times 184 \text{ rad s}^{-1}, \omega_z^{987} = 2\pi \times 122 \text{ rad s}^{-1}\}$ . We observe all three centre-of-mass degrees-of-freedom due to imperfect alignment between the coordinate axis of the Paul trap and our imaging system. The additional frequency components in the spectrum for ID 987 could be other degrees-of-freedom (e.g. librational) or evidence of multi-particle collective modes, but that is beyond the scope of this study.

The EBC is not limited to tracking two particles, and in fig. 5(c) we show that the GTA has identified 5 separate particles. Due to varying  $Q/m$ , each particle has different resonant motional frequencies, and hence it is possible to individually excite them. We believe this opens the door to the study of a wide range of non-equilibrium phenomena.

## 5. Conclusion

In conclusion, we have shown that event-based imaging (EBI) is an interesting alternative to conventional detection schemes used for tracking levitated particles. The key enabling feature of EBI is the low data transfer, which enables event-based cameras (EBC) to track multiple objects at higher speeds than conventional cameras, and when combined with natural low pixel latencies [19] will allow the experimenter to implement real-time feedback for state control. As compared to photodiode-based detection schemes, EBCs feature a dynamic region of interest, enabling tracking over a wide field-of-view, with particular application in the study of non-equilibrium physics. We have demonstrated tracking over tens of micrometres whilst retaining 10 nm resolution. Finally, we have introduced an imaging technique suitable for fast tracking of a large number of particles, we believe at MHz rates with the application of tailored particle tracking algorithms.

## Acknowledgements

JM would like to thank Dr. John Dale for the inspiration to start this project. This research has been supported by the European Research Council (ERC) under the European Union's Horizon 2020 research and innovation programme (Grant Agreement Nos. 803277 & 957463) and by EPSRC New Investigator Award EP/S004777/1.

## Bibliography

- [1] J. Millen, T. S. Monteiro, R. Pettit, and A. N. Vamivakas, “Optomechanics with levitated particles,” *Rep. Prog. Phys.*, vol. 83, no. 2, p. 026401, 2020.

- [2] C. Gonzalez-Ballester, M. Aspelmeyer, L. Novotny, R. Quidant, and O. Romero-Isart, “Levitodynamics: Levitation and control of microscopic objects in vacuum,” *Science*, vol. 374, no. 6564, p. eabg3027, 2021.
- [3] J. Millen and B. A. Stickler, “Quantum experiments with microscale particles,” *Contemporary Physics*, vol. 61, no. 3, pp. 155–168, 2020.
- [4] J. Millen and J. Gieseler, *Single Particle Thermodynamics with Levitated Nanoparticles*, pp. 853–885. Cham: Springer International Publishing, 2018.
- [5] M. Rademacher, J. Millen, and Y. L. Li, “Quantum sensing with nanoparticles for gravimetry: when bigger is better,” *Advanced Optical Technologies*, vol. 9, no. 5, pp. 227–239, 2020.
- [6] D. C. Moore and A. A. Geraci, “Searching for new physics using optically levitated sensors,” *Quantum Science and Technology*, vol. 6, p. 014008, jan 2021.
- [7] T. Li, S. Kheifets, D. Medellin, and M. G. Raizen, “Measurement of the instantaneous velocity of a brownian particle,” *Science*, vol. 328, no. 5986, pp. 1673–1675, 2010.
- [8] V. Svák, J. Flajšmanová, L. Chvátal, M. Šiler, A. Jonáš, J. Ježek, S. H. Simpson, P. Zemánek, and O. Brzobohatý, “Stochastic dynamics of optically bound matter levitated in vacuum,” *Optica*, vol. 8, pp. 220–229, Feb 2021.
- [9] J. Ahn, Z. Xu, J. Bang, Y.-H. Deng, T. M. Hoang, Q. Han, R.-M. Ma, and T. Li, “Optically levitated nanodumbbell torsion balance and ghz nanomechanical rotor,” *Phys. Rev. Lett.*, vol. 121, p. 033603, Jul 2018.
- [10] R. Reimann, M. Doderer, E. Hebestreit, R. Diehl, M. Frimmer, D. Windey, F. Tebbenjohanns, and L. Novotny, “Ghz rotation of an optically trapped nanoparticle in vacuum,” *Phys. Rev. Lett.*, vol. 121, p. 033602, Jul 2018.
- [11] L. Magrini, P. Rosenzweig, C. Bach, A. Deutschmann-Olek, S. G. Hofer, S. Hong, N. Kiesel, A. Kugi, and M. Aspelmeyer, “Real-time optimal quantum control of mechanical motion at room temperature,” *Nature*, vol. 595, pp. 373–377, Jul 2021.
- [12] J. Gieseler, B. Deutscher, R. Quidant, and L. Novotny, “Subkelvin parametric feedback cooling of a laser-trapped nanoparticle,” *Phys. Rev. Lett.*, vol. 109, p. 103603, Sep 2012.
- [13] N. P. Bullier, A. Pontin, and P. F. Barker, “Super-resolution imaging of a low frequency levitated oscillator,” *Review of Scientific Instruments*, vol. 90, no. 9, p. 093201, 2019.
- [14] Y. Minowa, K. Kato, S. Ueno, T. W. Penny, A. Pontin, M. Ashida, and P. F. Barker, “Imaging based feedback cooling of a levitated nanoparticle,” 2022.
- [15] J. Millen, T. Deesawan, P. Barker, and J. Anders, “Nanoscale temperature measurements using non-equilibrium brownian dynamics of a levitated nanosphere,” *Nature Nanotechnology*, vol. 9, pp. 425–429, Jun 2014.
- [16] V. Jain, J. Gieseler, C. Moritz, C. Dellago, R. Quidant, and L. Novotny, “Direct measurement of photon recoil from a levitated nanoparticle,” *Phys. Rev. Lett.*, vol. 116, p. 243601, Jun 2016.
- [17] G. Afek, D. Carney, and D. C. Moore, “Coherent scattering of low mass dark matter from optically trapped sensors,” *Phys. Rev. Lett.*, vol. 128, p. 101301, Mar 2022.
- [18] H. Rudolph, U. Delić, M. Aspelmeyer, K. Hornberger, and B. A. Stickler, “Force-gradient sensing and entanglement via feedback cooling of interacting nanoparticles,” 2022.
- [19] G. Gallego, T. Delbrück, G. Orchard, C. Bartolozzi, B. Taba, A. Censi, S. Leutenegger, A. J. Davison, J. Conradt, K. Daniilidis, and D. Scaramuzza, “Event-based vision: A survey,” *IEEE Trans. Pattern Anal. Mach. Intell.*, vol. 44, pp. 154–180, Jan. 2022.
- [20] “Event-based vision whitepaper.” <https://www.prophesee.ai/whitepaper-download>. Accessed: 2022-06-17.
- [21] D. S. Bykov, P. Mestres, L. Dania, L. Schmöger, and T. E. Northup, “Direct loading of nanoparticles under high vacuum into a paul trap for levitodynamical experiments,” *Applied Physics Letters*, vol. 115, no. 3, p. 034101, 2019.
- [22] M. Nikkhou, Y. Hu, J. A. Sabin, and J. Millen, “Direct and clean loading of nanoparticles into optical traps at millibar pressures,” *Photonics*, vol. 8, no. 11, 2021.
- [23] I. A. Martinez, É. Roldán, L. Dinis, and R. A. Rica, “Colloidal heat engines: a review,” *Soft matter*,

- vol. 13, no. 1, pp. 22–36, 2017.
- [24] M.-T. Wei and H. D. Ou-Yang, “Thermal and non-thermal fluctuations of the mechanical properties in living cells,” in *Optical Trapping and Optical Micromanipulation VII*, vol. 7762, p. 77621L, International Society for Optics and Photonics, 2010.
  - [25] I. A. Martinez, É. Roldán, L. Dinis, P. Mestres, J. M. Parrondo, and R. A. Rica, “Stochastic thermodynamics with a brownian particle in an optical trap (presentation recording),” in *Optical Trapping and Optical Micromanipulation XII*, vol. 9548, p. 954816, International Society for Optics and Photonics, 2015.
  - [26] L. Rondin, J. Gieseler, F. Ricci, R. Quidant, C. Dellago, and L. Novotny, “Direct measurement of kramers turnover with a levitated nanoparticle,” *Nature nanotechnology*, vol. 12, no. 12, pp. 1130–1133, 2017.
  - [27] Y. Jun, M. Gavrilov, and J. Bechhoefer, “High-precision test of landauer’s principle in a feedback trap,” *Physical review letters*, vol. 113, no. 19, p. 190601, 2014.
  - [28] T. M. Hoang, R. Pan, J. Ahn, J. Bang, H. Quan, and T. Li, “Experimental test of the differential fluctuation theorem and a generalized jarzynski equality for arbitrary initial states,” *Physical review letters*, vol. 120, no. 8, p. 080602, 2018.
  - [29] Z. Wang, Y. Ng, C. Scheerlinck, and R. Mahony, “An asynchronous kalman filter for hybrid event cameras,” in *Proceedings of the IEEE/CVF International Conference on Computer Vision*, pp. 448–457, 2021.
  - [30] S. Afshar, A. P. Nicholson, A. van Schaik, and G. Cohen, “Event-based object detection and tracking for space situational awareness,” *IEEE Sensors Journal*, vol. 20, no. 24, pp. 15117–15132, 2020.
  - [31] S. Kotler, G. A. Peterson, E. Shojaee, F. Lecocq, K. Cicak, A. Kwiatkowski, S. Geller, S. Glancy, E. Knill, R. W. Simmonds, *et al.*, “Direct observation of deterministic macroscopic entanglement,” *Science*, vol. 372, no. 6542, pp. 622–625, 2021.
  - [32] I. Brandão, D. Tandeitnik, and T. Guerreiro, “Coherent scattering-mediated correlations between levitated nanospheres,” *Quantum Science and Technology*, vol. 6, no. 4, p. 045013, 2021.
  - [33] L. Mercier de Lépinay, C. F. Ockeloen-Korppi, M. J. Woolley, and M. A. Sillanpää, “Quantum mechanics-free subsystem with mechanical oscillators,” *Science*, vol. 372, no. 6542, pp. 625–629, 2021.
  - [34] T. Roque and J. Roversi, “Quantum correlations between two oscillators connected by a time-dependent coupling,” in *Latin America Optics and Photonics Conference*, pp. LS2B-2, Optical Society of America, 2012.
  - [35] L. Qi, Y. Xing, S. Liu, S. Zhang, and H.-F. Wang, “Topological phase induced by distinguishing parameter regimes in a cavity optomechanical system with multiple mechanical resonators,” *Physical Review A*, vol. 101, no. 5, p. 052325, 2020.
  - [36] D. Carney, G. Krnjaic, D. C. Moore, C. A. Regal, G. Afek, S. Bhave, B. Brubaker, T. Corbitt, J. Cripe, N. Crisosto, *et al.*, “Mechanical quantum sensing in the search for dark matter,” *Quantum Science and Technology*, vol. 6, no. 2, p. 024002, 2021.
  - [37] D. C. Moore and A. A. Geraci, “Searching for new physics using optically levitated sensors,” *Quantum Science and Technology*, vol. 6, no. 1, p. 014008, 2021.
  - [38] R. Zhao, A. Manjavacas, F. J. G. de Abajo, and J. Pendry, “Rotational quantum friction,” *Physical Review Letters*, vol. 109, no. 12, p. 123604, 2012.
  - [39] H. Rudolph, U. Delić, M. Aspelmeyer, K. Hornberger, and B. A. Stickler, “Force-gradient sensing and entanglement via feedback cooling of interacting nanoparticles,” *arXiv preprint arXiv:2204.13684*, 2022.
  - [40] T. Penny, A. Pontin, and P. Barker, “Sympathetic cooling and squeezing of two co-levitated nanoparticles,” *arXiv preprint arXiv:2111.03123*, 2021.
  - [41] J. Rieser, M. A. Ciampini, H. Rudolph, N. Kiesel, K. Hornberger, B. A. Stickler, M. Aspelmeyer, and U. Delić, “Observation of strong and tunable light-induced dipole-dipole interactions between optically levitated nanoparticles,” *arXiv preprint arXiv:2203.04198*, 2022.

- [42] Y. Arita, E. M. Wright, and K. Dholakia, “Optical binding of two cooled micro-gyrosopes levitated in vacuum,” *Optica*, vol. 5, no. 8, pp. 910–917, 2018.
- [43] B. R. Slezak and B. D’Urso, “A microsphere molecule: The interaction of two charged microspheres in a magneto-gravitational trap,” *Applied Physics Letters*, vol. 114, no. 24, p. 244102, 2019.
- [44] J. Vijayan, Z. Zhang, J. Piotrowski, D. Windey, F. van der Laan, M. Frimmer, and L. Novotny, “Scalable all-optical cold damping of levitated nanoparticles,” *arXiv preprint arXiv:2205.04455*, 2022.
- [45] P. Praveen, S. S. Iyengar, S. Bhattacharya, S. Ananthamurthy, *et al.*, “Two particle tracking and detection in a single gaussian beam optical trap,” *Applied Optics*, vol. 55, no. 3, pp. 585–594, 2016.
- [46] G. M. Gibson, J. Leach, S. Keen, A. J. Wright, and M. J. Padgett, “Measuring the accuracy of particle position and force in optical tweezers using high-speed video microscopy,” *Optics express*, vol. 16, no. 19, pp. 14561–14570, 2008.
- [47] D. Ott, S. Nader, S. Reihani, and L. B. Oddershede, “Simultaneous three-dimensional tracking of individual signals from multi-trap optical tweezers using fast and accurate photodiode detection,” *Optics express*, vol. 22, no. 19, pp. 23661–23672, 2014.

## Supplementary Information

### Appendix A. Calibration: Solving for $Q/m$

Considering that our system follows a Mathieu equation of motion then the frequency of the different degrees of motion can be written as,

$$\omega_i \cong \frac{1}{2}\Omega\sqrt{a_i + \frac{1}{2}q_i^2}, \quad (\text{A.1})$$

where  $\omega_i$  the harmonic oscillation frequency and  $a_i, q_i$  with  $i = x, y, z$  are known as the stability parameters.

Using the stability parameters we can write a general statement for all three axis:

$$\omega_i^2 = q_m^2 \left( \frac{V_R F^2}{2\Omega_{RF}^2 r^4} \alpha_i^2 \right) + q_m \left( \frac{2U}{d^2} \right) \beta_i. \quad (\text{A.2})$$

where we  $q_m = Q/M$  and is the charge-mass ratio,  $\Omega_{RF}$  is the RF frequency,  $V_{RF}$  is the RF voltage amplitude,  $U$  is the DC voltage at the endcaps,  $r$  is the distance between RF electrodes from the centre of the trap and  $d$  is the distance between the endcap electrodes. The variables  $\alpha_i$  and  $\beta_i$  are geometric factors that are obtained through SIMION numerical simulation of the Paul trap used in the experiments (see Table A1) for each axis,  $i \in \{x, y, z\}$ .

	x	y	z
$\alpha$	2.32	3.74	6.37
$\beta$	-0.090	-0.090	-0.198

Table A1: Geometric factors obtained from SIMION numerical simulation of the Paul Trap

The  $Q/m$  ratio can then be obtained by solving for  $q_m$  of the three simultaneous equations.

### Appendix B. Calibration: Nonlinear Calibration with the QPD

To calibrate the system and obtain a conversion function we apply an electric force,  $F_E$  to the particle via the endcap electrodes:

$$F_E = \frac{qU}{d}, \quad (\text{B.1})$$

which is equal to spring force experienced in the trap:  $m\omega^2\bar{x}$ . When equated with the above equation we get a theoretical value for positional shift in metres for an applied voltage  $U$ :

$$\bar{x}_m = \frac{Q}{m} \frac{U}{\omega_0^2 d}. \quad (\text{B.2})$$

The quadrant photodetector (QPD) has a nonlinear response to the movement of an image if the image deviates too far from the centre, i.e. if the particle moves too far from the centre of the trap. We can fit an error function to the mean position of the particle (recorded in Volts),  $\tilde{x}_V$ , with the expected shift in  $\tilde{x}_m$  based on the amount of voltage being applied, Eq B.2.

$$\tilde{x}_V = a + b * \operatorname{erf}\left(\frac{\bar{x}_m - c}{d}\right) \quad (\text{B.3})$$

where  $(a, b, c, g)$  are fitting constants obtained by fitting the above equation to the data as shown in fig. B1. The inverse of this error function then enables us to convert the positional information in volts  $x_V(t)$  to metres  $x_m(t)$ .

$$x_m(t) = g \operatorname{erf}^{-1}\left(\frac{x_V(t) - a}{b}\right) + c, \quad (\text{B.4})$$

This enables us to extend the detection range of the QPD by a few microns, but not by the tens of microns offered by the event-based camera.

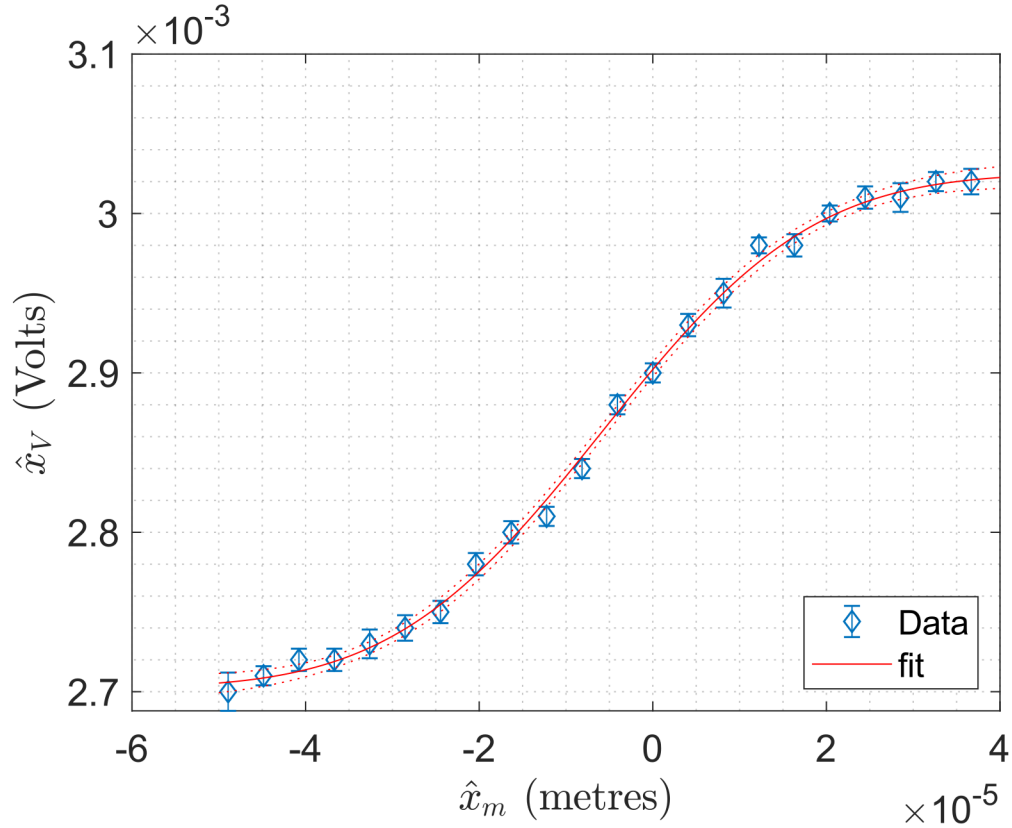


Figure B1: Caption

### Appendix C. Generating Random Jumps

Random jumps in position of the particle are implemented by applying telegraph noise statistics to the particle. To achieve this, we generate random numbers normally distributed, which then are multiplied by a mean waiting time  $\bar{\tau}$ . The waiting time is then used to delay a voltage applied to the particle  $\pm V_{tel}$  via the endcap electrodes. This applied voltage is experienced by the trapped particle as an electric force,  $\pm \eta_{tel} = \frac{Q}{m} V_{tel}/(d)$ . In this work,  $V_{tel} = \pm 1$  V.

This applied force has noise statistics governed by:

$$\langle \eta_t \eta_{t'} \rangle = \eta_{tel}^2 e^{(-2|t-t'|/\tau)} \quad (\text{C.1})$$